ELSEVIER

Journal of Nuclear Materials 280 (2000) 365–371

journal of nuclear materials

www.elsevier.nl/locate/jnucmat

Phase transition temperature in the Zr-rich corner of Zr–Nb–Sn–Fe alloys

M. Canay *, C.A. Danón, D. Arias

Departamento de Materiales, Centro Atómico Constituyentes, Comisión Nacional de Energía Atómica, Av. del Libertador 8250, 1429 Buenos Aires, Argentina

Received 7 July 1999; accepted 20 March 2000

Abstract

The influence of small composition changes on the phase transformation temperature of Zr–1Nb–1Sn–0.2(0.7)Fe alloys was studied in the present work, by electrical resistivity measurements and metallographic techniques. For the alloy with 0.2 at.% Fe we have determined $T_{\alpha\leftrightarrow\alpha+\beta} = 741°C$ and $T_{\alpha+\beta\leftrightarrow\beta} = 973°C$, and for the 0.7 at.% Fe the transformation temperatures were $T_{\alpha\leftrightarrow\alpha+\beta} = 712°C$ and $T_{\alpha+\beta\leftrightarrow\beta} = 961°C$. We have verified that the addition of Sn stabilized the β phase.

PACS: 81.30.Bx

1. Introduction

Some zirconium alloys are generally used as cladding and structural materials in light and heavy water nuclear reactors, due to their excellent neutron economy and corrosion resistance. We have decided to carry out an investigation of the transformation temperatures on one of them, the Zr–1Nb–1Sn–0.1Fe (wt%) alloy known as ZIRLO (Westinghouse Electric Corp. trade mark). Pure zirconium at atmospheric pressure has a body-centered cubic structure (β) from 865°C to the liquidus, a hexagonal close packed structure (α) from 865°C to 0 K and a hexagonal ω phase at high pressure [1,2]. The α/β boundary is modified by the addition of alloying elements as illustrated in the case of the Zircaloy alloys, where a two-phase region at approximately 200°C was measured [3,4]. The ternary ZrNbSn system was studied in 1958 by Ivanov and Grigorovich [5] who presented isothermal sections at 1050°C, 940°C, 850°C, 725°C, and 500°C from microstructural and X-ray analysis of samples in the Zr-rich region of the diagram with a Sn content up to 10 at.% and Nb up to 30 at.% and after measuring microhardness suggested that the Sn addition in Zr–Nb would stabilize the β-phase. Later, in 1990 Korotkova [6] studied this part of the phase diagram again and presented isothermal sections at 1000°C, 940°C, 900°C, 800°C and 720°C which do not contradict Ivanov and Grigorovich results [5].

From the observations made in three different alloys (Zr–1.17Sn–1Nb–0.20Fe wt%, Zr–1.36Sn–0.97Nb–0.33Fe wt% and Zr–1.20Sn–1.10Nb–0.46Fe wt%) Markelov et al. [7] in 1994 identified two different kinds of precipitates, $ZrFe_3$ and $Zr(NbFe)_2$ of approximately 1 and 0.1 μm in size, respectively. Regarding the phase transformation temperatures, Curtis and Dressler [8] reported that the addition of 1%Sn in the ZrNb system has two different effects: (a) increases by 28°C the β transformation temperature; (b) diminishes the Nb solubility in Zr(α). Recently, Niculina et al. [9] published a paper in which they describe the evolution of the microstructure in the Zr–1Nb–1Sn–0.4Fe (wt%) alloys under irradiation. They suggested that the phase transformation temperature $\alpha \leftrightarrow \alpha + \beta$ is about 650°C, and they also find the $(ZrNb)_3Fe$, $Zr(NbFe)_2$ and Zr_4Sn precipitates. Niculin et al. [10] indicated also that the $\alpha + \beta/\beta$ boundary is located at 950°C in the same alloy. More recently, Toffolon et al. [11] reported a thermogram obtained by calorimetry during the cooling of a

* Corresponding author. Fax: +5-411 4754 7362.
E-mail address: mcanay@cvtci.com.ar (M. Canay).

0022-3115/00/$ - see front matter
PII: S0022-3115(00)00050-7

sample corresponding to Zr–1Nb–1Sn–0.5Fe (wt%) alloy. In the thermogram, they identified a secondary phase precipitation temperature of about 650°C.

The present investigation will focus on the $\alpha \leftrightarrow \beta$ phase transformation temperature corresponding to Zr–1Nb–0.8Sn–0.2(0.7)Fe (at.%) alloys by means of electrical resistivity vs temperature measurements supplemented by metallography and microprobe analysis. We will also consider the effect of small composition changes (Sn, Nb, Fe) on the phase transformation temperature.

2. Experimental

Eight ingots (≈10 g) were prepared in an arc furnace with a *W* electrode and a cooling copper crucible, in a high purity argon atmosphere (1 at ppm impurity). The starting materials were (99.999%) Sn, (99.99%) Nb, and (99.8%-nuclear grade) Zr. The Zr–1Nb (wt%) and Zr–2.5Nb (wt%), (nuclear quality), have also been studied for the sake of comparison. The chemical composition of the alloys is given in Table 1.

Each sample was cold-rolled in three steps with intermediate heat-treatments 750°C (24 h) down to 2 mm for metallographic studies and to 0.2 mm for resistivity measurements. For the different heat treatments, the samples were mechanically polished, chemically etched with different mixtures of HF, HNO_3 and H_2O (5:45:50), carefully rinsed in distilled water, cleaned in hot ether, wrapped in clean tantalum foil and sealed in a silica glass tube with a high-purity argon (1 at ppm impurities) atmosphere.

Different isothermal heat treatments were carried out on the different alloys. In all the cases, we have first β homogenized the samples during a minimum of 12 h at 1050°C. This treatment was followed by cooling to the selected isothermal annealing temperature, after which the samples were finally water quenched to room temperature.

Electrical resistivity measurements were used to determine the α/β phase boundaries. The experimental arrangement for the high-temperature measurements consisted of a silica glass tube (containing the sample) connected to a high-vacuum system ($\leqslant 10^{-4}$ Pa). Polycrystalline strips, $3 \times 0.2 \times 30$ mm were provided with four spot-welded Zr–1Nb (wt%) wires for the current–voltage measurements. The temperature of the samples was measured with a Pt/Pt − 10 wt% Rh calibrated thermocouple, with its measuring point joint carefully located to avoid contact with the silica glass tube wall, and in the same isothermal section as the sample. Voltage and external resistance setting were chosen to maintain a constant current through the samples, so that the output from the voltage taps was directly proportional to the resistivity (Fig. 1). The samples were heated and cooled at controlled rates (3°C/min).

Optical micrographs were obtained under polarized light. Heat-treated samples were also observed by scanning electron microscopy (SEM) in a Philips PSEM-500 instrument. The compositions were determined by electron microanalysis (Cameca SX50) microprobe operated at 20 kV with an electron beam current of 20 nA, and a chamber vacuum of 2×10^{-4} Pa. Prior to optical, SEM and electron microanalysis, the samples were

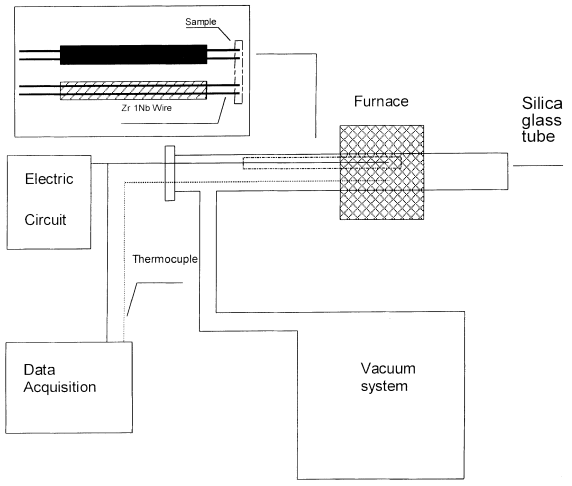

Fig. 1. Electrical resistivity device.

Table 1
Chemical composition of materials (Zr balance)

	Alloy	Nb (at.%)	Nb (wt%)	Sn (at.%)	Sn (wt%)	Fe (at.%)	Fe (wt%)	Cr (at.%)	Cr (wt%)
1	Zr–1Nb–0.8Sn–0.2Fe	1.0	1.0	0.8	1.0	0.2	0.1	–	–
2	Zr–1Nb–0.8Sn–0.7Fe	1.0	1.0	0.8	1.0	0.7	0.4	–	–
3	Zr–2.4Nb–3.1Sn	2.4	2.4	3.1	4.0	0.2	0.1	–	–
4	Zr–3Nb–0.8Sn	3.0	3.0	0.8	1.0	0.2	0.1	–	–
5	Zr–1Nb–1.6Sn	1.0	1.0	1.6	2.1	0.2	0.1	–	–
6	Zr–1Nb	1.0	1.0	–	0.0	0.2	0.1	–	–
7	Zr–2.5Nb	2.5	2.5	–	0.0	0.2	0.1	–	–
8	Zr–1Nb–0.7Sn–0.4(Fe + Cr)	1.0	1.0	0.7	0.9	0.3	0.2	0.1	0.05

ground on silicon carbide paper, polished with diamond paste (7 and 1 μm) and etched using a mixture of HF, HNO_3 and distilled water. Crystallographic structures were identified using monochromatic Cu Kα radiation at room temperature in a Philips PW3HO X-ray diffractometer.

3. Results and discussion

3.1. Transformation temperatures

The transformation temperatures of the eight alloys determined by the variation of the electrical resistivity vs temperature are presented in Table 2. The samples were either heated or cooled at a rate of 3°C/min from room temperature up to 1100°C. (Fig. 2). After each electrical resistivity experiment, the maximum resistivity value in the run was selected (ρ_0) and was used for normalization. ρ/ρ_0 vs T was represented in each graph.

We have measured each sample twice in order to study the influence of the oxygen on the transformation temperature. The oxygen concentration increases by about 1450 at ppm (~250 wt ppm) per heating and cooling run [12]. We have thus verified that the inevitable addition of this interstitial element affects the transformation temperatures in a different way, in the case of $\alpha \leftrightarrow \alpha+\beta$ or $\alpha+\beta \leftrightarrow \beta$ transformations. We will now analyze in more detail the way in which transformation temperatures of the alloys Zr–1Nb–0.8Sn–0.2(0.7)Fe are affected by the heating and cooling experiments (Table 3). The $\alpha \leftrightarrow \alpha+\beta$ temperatures in all the runs are quite similar. The $\alpha+\beta \leftrightarrow \beta$ temperatures obtained in the successive runs differ considerably, due to the incorporation of oxygen. These alloys exhibit hysteresis in the $\beta \rightarrow \alpha$ transformation temperature, as it was observed in other Zr alloy system [13]. Consequently the criteria used in order to determine these temperatures in each case were:

1. The $T_{\alpha \leftrightarrow \alpha+\beta}$ temperature as determined by our heating and cooling resistivity measurement were slightly different. This is the reason why we decided to take the average of the measured temperatures of the heating run ($\alpha \rightarrow \alpha+\beta$) and the cooling run ($\alpha+\beta \rightarrow \alpha$).
2. The $T_{\alpha+\beta \leftrightarrow \beta}$ temperature was substantially altered and in this case we have chosen the temperature which corresponds to the first heating run, where the oxygen contamination was minimum.

'Resistivity' transformation temperatures are those for which $d\rho/dT = 0$; ($\rho = a + bT + cT^2 + dT^3$).

At this stage, it must be remembered that, as pointed out by Mooij [14], the electrical resistivity of highly resistive systems (like Zr) does not obey Matthiessen's rule

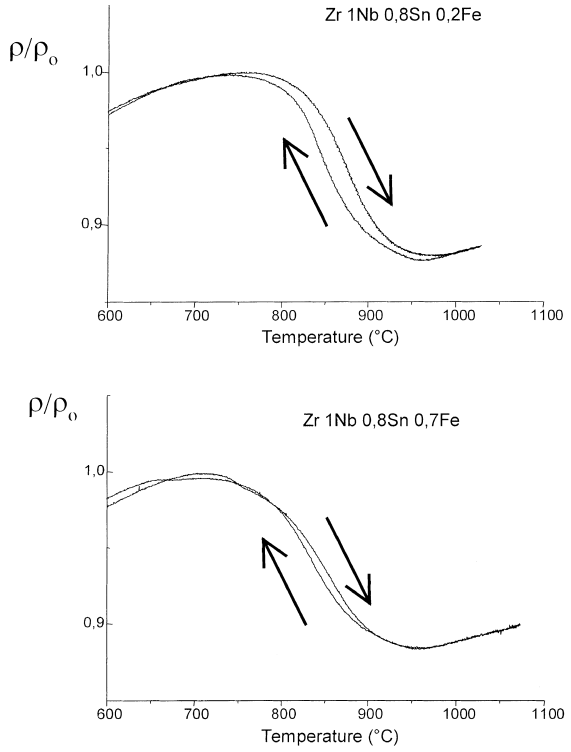

Fig. 2. Resistivity (ρ) vs temperature (T) measurements.

Table 2
$\alpha \leftrightarrow \beta$ transformation temperatures as obtained from electrical resistivity measurements

	Alloy	$\alpha \leftrightarrow \alpha+\beta$ (°C)	$\alpha+\beta \leftrightarrow \beta$ (°C)
1	Zr–1Nb–0.8Sn–0.2Fe	741	973
2	Zr–1Nb–0.8Sn–0.7Fe	712	961
3	Zr–2.4Nb–3.1Sn	568	980
4	Zr–3Nb–0.8Sn	670	910
5	Zr–1Nb–1.6Sn	730	1000
6	Zr–1Nb	776	948
7	Zr–2.5Nb	700	920
8	Zr–1Nb–0.7Sn–0.4(Fe + Cr)	707	975

V: heating and cooling 3°C/min

Table 3
$\alpha \leftrightarrow \beta$ transformation temperatures in the Zr–1Nb–0.8Sn–0.2(0.7)Fe alloys, as measured twice by electrical resistivity

		Run	$\alpha \rightarrow \alpha+\beta$	$\alpha+\beta \rightarrow \alpha$	$\alpha+\beta \rightarrow \beta$	$\beta \rightarrow \alpha+\beta$
1	Zr–1Nb–0.8Sn–0.2Fe	1	744	739	973	962
		2	742	739	994	981
2	Zr–1Nb–0.8Sn–0.7Fe	1	712	713	975	967
		2	713	711	996	978

Table 4
Heat treatments

Alloys	High α	Low $(\alpha+\beta)$
Zr–1Nb–0.8Sn–0.2Fe	720°C (14 days)	770°C (14 days)
Zr–1Nb–0.8Sn–0.7Fe	690°C (14 days)	730°C (14 days)

and the ρ vs T curves for the hcp phases show an upward curve which is usually reported as resistivity saturation [15]. This effect is more pronounced in some Zr alloys like Zr–O [16], Zr–Sn [17,18], Zr–1Nb [19]. In those materials, in which the ρ vs T curve is almost lineal at temperature very near the transformation temperature, the latter can be determined by lineal extrapolation of the last portion of the curve. This is not the case of the present work, and that is why we have made a cubic polynomial fit of the experimental data and used the $d\rho/dT = 0$ criterion for the transformation temperature. This choice was possible since: (1) our alloys show no negative temperature dependence of resistivity in the α and β phases; (2) $\rho_\alpha > \rho_\beta$; $\rho_\alpha/\rho_\beta = 1.2$ for the pure Zr [20,21] and $\rho_\alpha/\rho_\beta = 1.14$ in our experiments, thus ρ is a property very sensitive to precipitation of either phases; (3) the $d\rho/dT = 0$ criterion has been applied in previous works [13,22,23]; (4) the same criterion was verified by metallography as well.

3.2. Zr–1Nb–0.8Sn–0.2(0.7)Fe (at.%) alloy

In order to verify the $d\rho/dT = 0$ criterion, long-term (336 h) heat treatments below and above the $\alpha/\alpha+\beta$ boundary were made on both alloys (Table 4).

Metallography of these alloys showed the typical Zircaloy Widmanstätten morphology, but with some small changes in the microstructure when the samples were in the low $(\alpha+\beta)$ field. Quantitative microprobe analysis of these samples showed an inhomogeneous distribution of Zr, Nb, Sn and Fe. As an example, Fig. 3(a) shows the Fe increase in the Widmanstatten interplates ($\approx$1 μm wide) in a sample heat treated in the α field (690°C). Fig. 3(b) shows the same Widmanstatten interplates Fe content, plus a $\approx$10 μm wide zones which were β phase at 730°C, with high concentration of Fe as well. Within β phase zones we have measured the compositions 5 at.% Nb, 3.5 at.% Fe, 0.3 at.% Sn, Zr (balance).

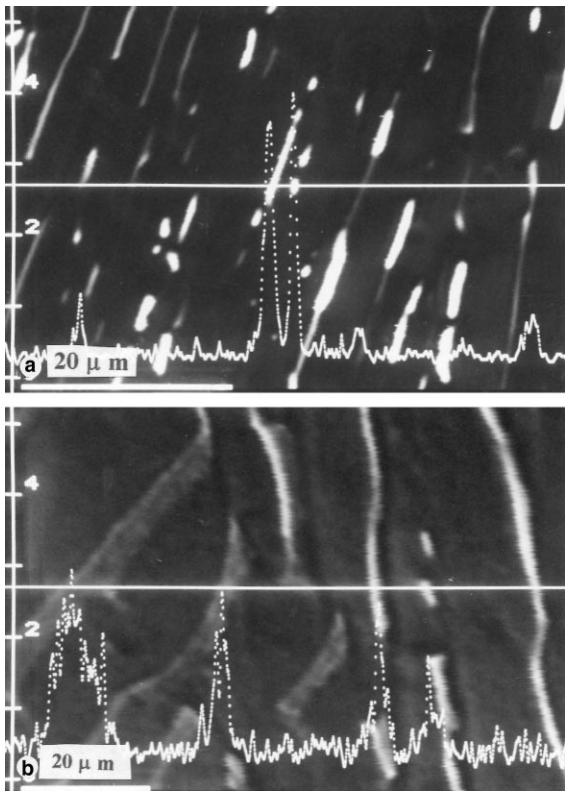

Fig. 3. Backscattered electron micrographs corresponding to the Zr–1Nb–0.8Sn–0.7Fe alloy and the variation of the Fe content in a lineal section of the samples: (a) β heat treated at 1050°C (24 h) and cooled to the isothermal annealing temperature at 690°C (336 h) (α phase); (b) β heat treated at 1050°C (24 h) and cooled to the isothermal annealing temperature at 730°C (336 h) ($\alpha+\beta$ phase) (line 20 μm).

With respect to the temperatures measured in this study, we want to emphasize that: (1) the phase transition temperatures corresponding to the alloy with

0.2 at.% Fe (close to ZIRLO) was $T_{\alpha\leftrightarrow\alpha+\beta} = 741°C$, and $T_{\alpha+\beta\leftrightarrow\beta} = 973°C$; (2) the temperatures corresponding to the alloy with 0.7% Fe was $T_{\alpha\leftrightarrow\alpha+\beta} = 712°C$, significantly different from the temperature measured by Niculina et al. [9] ($T_{\alpha\leftrightarrow\alpha+\beta} = 650°C$). Taking into account the above-mentioned paper of Toffolon et al. [11] we can assume that the temperature measured by Niculina et al. [9] corresponds to the formation of some intermetallic precipitates. The transformation temperature $T_{\alpha+\beta\leftrightarrow\beta} = 961°C$ which is slightly different from the temperature measured by Niculin et al. [10], could be attributed to small differences in the O content.

In Table 5, we show the microstructure and composition of both alloys after being heat treated at 800°C (710 h) and 850°C (760 h). From these results we can conclude that:

1. the solubility of Nb and Fe in the α phase was almost zero (less than 0.1 at.%);
2. the solubility of Nb in the β phase and the Sn solubility in the α and β phases were consistent with the behavior in the ZrSn [24] and ZrNb [25] binary phase diagrams and with the relative quantity of these phases present in the samples. We have estimated, as a first approach, the α/β ratio at different temperatures from the ρ vs T curves (Fig. 2).

Fig. 4 shows the $(\alpha + \beta)$ structure at 850°C (760 h), where the high temperature α-plates have grown in the β matrix and where β regions were transformed into α-Widmanstatten during the cooling from 850°C to room temperature. According to the metallography, the alloy with higher Fe content behaves in a similar way as the one described above, the only difference being the α/β ratio.

3.3. Zr–xNb–ySn–0.2Fe (at.%) alloy

In order to study the influence of small changes in the Nb and Sn composition, we have prepared three alloys

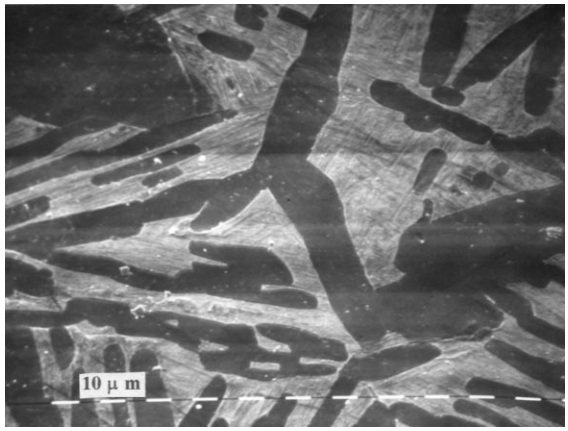

Fig. 4. Scanning electron microscopy observation of Zr–1Nb–0.8Sn–0.2Fe. Water quenching after β-homogenization 1050°C (1 h), and cooling to the isothermal annealing temperature at 850°C (760 h) (10 μm).

($x = 2.4 - 3 - 1$; and $y = 3.1 - 0.8 - 1.6$, respectively). We have determined the $(\alpha + \beta)$ two-phase region from the ρ vs T experiments (Table 2).

We have measured the composition in both phases, with the electron microprobe, in the three alloys heat treated at 825°C (216 h) and 875°C (120 h) (Table 6). The analysis of our results suggests that:

1. the alloys Zr–3Nb–0.8Sn (at.%) and Zr–1Nb–1.6Sn (at.%) are located in the $(\alpha + \beta)$ two-phase region, Fe solubility being practically null in the α phase;
2. the alloy Zr–2.4Nb–3.1Sn (at.%) is located in the three-phase region ($\alpha + \beta +$ intermetallic). In the case of this alloy (with high Sn content and heat treated at 825°C), small precipitates were observed with a Sn/Fe ratio similar to the one reported by Tanner [26] for the θ phase. Therefore, the intermetallic is most probably the θ phase.

Table 5
Microstructure and chemical composition (Zr balance)

Alloy	800°C (710 h)		850°C (760 h)	
	Microstructure	Composition	Microstructure	Composition
Zr–1Nb–0.8Sn–0.2Fe	hcp	0.1 at.% Nb	hcp	0.0 at.% Nb
		0.8 at.% Sn		1.0 at.% Sn
		<0.1 at.% Fe		<0.1 at.% Fe
	bcc	3.2 at.% Nb	bcc	1.5 at.% Nb
		0.6 at.% Sn		0.6 at.% Sn
		0.9 at.% Fe		0.7 at.% Fe
Zr–1Nb–0.8Sn–0.7Fe	hcp	<0.1 at.% Nb	hcp	<0.1 at.% Nb
		0.8 at.% Sn		1.0 at.% Sn
		<0.1 at.% Fe		<0.1 at.% Fe
	bcc	2.3 at.% Nb	bcc	1.3 at.% Nb
		0.5 at.% Sn		0.6 at.% Sn
		2.8 at.% Fe		1.2 at.% Fe

Table 6
Microstructure and chemical composition (Zr balance)

Alloy	Heat treatment (°C, h)	Phase	Sn (at.%)	Nb (at.%)	Fe (at.%)
Zr–2.4Nb–3.1Sn	825 (216)[a]	hcp	3.5	0.3	<0.1
		bcc	2.2	5.0	0.1
	875 (120)	hcp	3.2	0.4	<0.1
		bcc	1.9	4.0	0.4
Zr–3Nb–0.8Sn	825 (216)	hcp	1.1	0.3	<0.1
		bcc	0.6	4.1	0.2
	875 (120)	hcp	3.4	0.7	<0.1
		bcc	0.6	3.5	0.2
Zr–1Nb–1.6Sn	825 (216)	hcp	1.8	0.3	<0.1
		bcc	1.1	3.6	0.5
	875 (120)	hcp	2.7	0.6	<0.1
		bcc	0.2	1.7	0.3
Zr–1Nb–0.7Sn–0.4(Fe + Cr)	850 (170)	hcp	0.8	0.1	<0.1 (Fe + Cr)
		bcc	0.4	2.5	2.0 (Fe + Cr)

[a] We observed some Zr Sn Fe small precipitates.

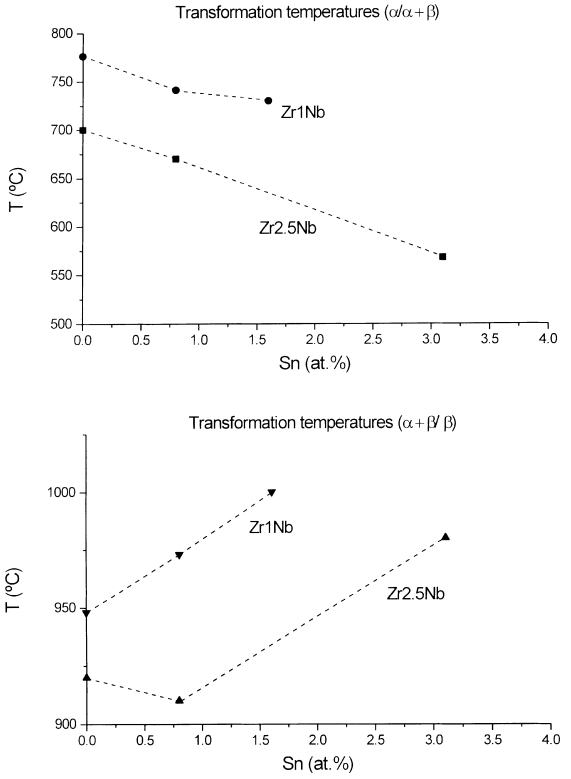

Fig. 5. Effect of Sn on the $T_{\alpha/\alpha+\beta}$ and $T_{\alpha+\beta/\beta}$ for Zr–1Nb and Zr–2.5Nb alloys.

Comparing the $\alpha \leftrightarrow \beta$ transformation temperatures measured in the alloys Zr–1Nb–1.6Sn and Zr–2.4Nb–3.1Sn, with the temperatures measured in the alloys Zr–1Nb and Zr–2.5Nb, respectively, we can conclude that:

1. the addition of Sn increases the $\alpha + \beta \leftrightarrow \beta$ phase transformation temperature, as expected [21];

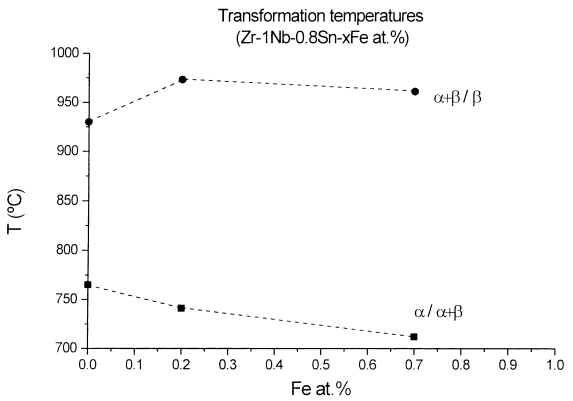

Fig. 6. Effect of Fe on the $T_{\alpha/\alpha+\beta}$ and the $T_{\alpha+\beta/\beta}$ for the Zr–1Nb–0.8Sn alloy.

2. with respect to the $\alpha \leftrightarrow \alpha + \beta$ phase transformation temperature, the addition of Sn stabilizes the β phase, as reported by Ivanov and Grigorovich [5].

Fig. 5 shows the effect of Sn on the $T_{\alpha\rightarrow\alpha+\beta}$ and the $T_{\alpha+\beta\rightarrow\beta}$ for Zr–1Nb and Zr–2.5Nb alloys. It should be remarked that the temperature obtained for the 0.8 at.% Sn corresponds to the Zr–3Nb–0.8Sn alloy; the difference in the transformation temperature is not considered to be significant.

Fig. 6 shows the effect of Fe on the $T_{\alpha\rightarrow\alpha+\beta}$ and the $T_{\alpha+\beta\rightarrow\beta}$ for the Zr–1Nb–0.8Sn alloy. The zero Fe content were extrapolated from the corresponding binary phase diagram [24,25,27].

3.4. Zr–xNb–ySn–z(Cr + Fe) (at.%) alloy

In some US Patent for instance [28,29] some possible alloys that could be obtained from Zircaloy's plus ZrNb

were proposed. In the present work, we have studied for the sake of comparison, one of those possible alloys. In Table 2, we can see the $\alpha \leftrightarrow \beta$ transformation temperature and in Table 6, we can see the average composition in a sample heat treated at 850°C (170 h).

The transformation temperatures and the chemical composition measured were similar to the corresponding Zr–1Nb–0.8Sn–0.7Fe (at.%). In the chemical composition, the only difference was the presence of Cr.

4. Conclusions

From the experimental results described in the present paper, we can conclude that:

The phase transformation temperatures were:

1. $T_{\alpha \leftrightarrow \alpha+\beta} = 741$°C, and $T_{\alpha+\beta \leftrightarrow \beta} = 973$°C, in the alloy Zr–1Nb–0.8Sn–0.2Fe;
2. $T_{\alpha \leftrightarrow \alpha+\beta} = 712$°C and $T_{\alpha+\beta \leftrightarrow \beta} = 961$°C, in the alloy Zr–1Nb–0.8Sn–0.7Fe;
3. we have also reported the changes in these temperatures which occur for small variations in composition;
4. the addition of Sn stabilizes the β phase.

Acknowledgements

This work was partially supported by CNEA-CAC (Grant PI&D 10/98) and CONICET-Argentina (Grant PIP 4040/96).

References

[1] J.P. Abriata, J.C. Bolcich, Bull. Alloy Phase Diagrams 3 (1) (1982) 28.
[2] A.F. Guillermet, High Temp.-High Press. 19 (1987) 119.
[3] A. Miquet, D. Charquet, C.H. Allibert, J. Nucl. Mater. 105 (1982) 132.
[4] D. Arias, R. Castillo Guerra, J. Nucl. Mater. 144 (1987) 196.
[5] O.S. Ivanov, V.K. Grigorovich, in: Proceedings of the Second UN International Conference PUAE, vol. 3, Geneva, 1958, p. 34.
[6] N.V. Korotkova, Russian Metall. (1990) 207.
[7] V.A. Markelov, V.Z. Rafikov, S.A. Nikulin, V.I. Goncharov, V.N. Shishov, A. YuGusev, E.K. Chesnokov, Phys. Met. Metallogr. 77 (1994) 380.
[8] R.E. Curtis, G. Dressler, Zirconium in Nuclear Applications, ASTM STP 551 (1974) 104.
[9] A.V. Niculina, V.A. Markelov, M.M. Peregud, V.N. Voevodin, V.L. Panchenko, G.P. Kobylyansky, J. Nucl. Mater. 238 (1996) 205.
[10] S.A. Niculin, M.A. Shtremel, V.A. Markelov, J. Phys. IV 6 (1996) C6–133.
[11] C. Toffolon, C. Servant, J.C. Brachet, J.P. Mardon, in: Proceedings of the 12th International Symposium on Zr in the Nuclear Industry, Toronto, Canada, Abstract, 15–18 June 1998, p. 97.
[12] M. Canay, D. Arias, 82 Anual Meeting of the Physical Association of Argentina, Anales AFA, 9, 1997, p. 280.
[13] D. Arias, M. Ruch, J.P. Abriata, Philos. Mag. A. 63 (5) (1991) 1103.
[14] J.H. Mooij, Phys. Status Solid (a) 17 (1973) 521.
[15] G. Grimvall, Rev. Int. Hautes Temp. Refract. 16 (1979) 411.
[16] E. Gebhardt, H.D. Seghezzi, W. Dürrschnabel, J. Nucl. Mater. 4 (3) (1961) 241.
[17] A. Goldsmith, T.E. Waterman, H.J. Hirshnorn, Handbook of Thermophysical Properties of Solid Materials VII: Alloys, MacMillan, New York, 1961, p. 703.
[18] L. Roberti, PhD dissertation, Buenos Aires University, 1992.
[19] V.E. Peletsky, Z.A. Musayeva, Int. J. Thermophys. 16 (6) (1995) 1481.
[20] P.D. Desai, H.M. James, C.Y. Ho, J. Phys. Chem. Ref. Data 13 (4) (1984) 1097.
[21] D. Arias, L. Roberti, J. Nucl. Mater. 118 (1983) 143.
[22] M. Ruch, D. Arias, Scripta Met. Mater. 29 (1993) 533.
[23] C. Angelier, S. Bein, J. Bêchet, Metall. Mater. Trans. A 28A (1997) 2467.
[24] J.P. Abriata, J.C. Bolcich, D. Arias, Bull. Alloy Phase Diagrams 4 (2) (1983) 147.
[25] H. Okamoto, J. Phase Equilib. 13 (5) (1992) 577.
[26] L.E. Tanner, D.W. Levinson, Trans. ASM 52 (1960) 1115.
[27] J.P. Abriata, J. Garces, R. Versaci, Bull. Alloy Phase Diagrams 7 (2) (1986) 116.
[28] J.P. Foster, et al., United States Patent No. 5112573, 12 May 1992.
[29] J.P. Foster, et al., United States Patent No. 5230758, 27 July 1993.